Journal of the Brazilian Society of Mechanical Sciences and Engineering manuscript No.
(will be inserted by the editor)

Numerical analysis of the influence of magnetic field waveforms on the performance of active magnetic regenerators

Fábio P. Fortkamp · Gusttav B. Lang · Jaime A. Lozano · Jader R. Barbosa Jr.

Abstract Keywords magnetic refrigeration · active magnetic regenerator · numerical modeling · magnetocaloric effect

1 Introduction

Mechanical vapor compression has been the dominant cooling technology for the past century [1] but, despite its dominance, it still faces an increasing number of challenges related to the its environmental footprint. The large entropy generation associated with vapor compression processes makes this techonology constrained by low exergy efficiencies, in particular for compact systems [2]. In addition, the phase-out of refrigerants with ozone depleting and global warming potentials has introduced the use of flammable substances, with their own set of risks for consumer applications [3] and technologial challenges [4].

The term *caloric cooling* is generally applied to alternative cooling techonologies in which the cooling effect is generated by the response of a solid material to a physical stimulus. The absence of hazardous gases, compressors and throttling devices makes these technologies potentially more efficient, scalable, silent and environmentally friendly. Magnetic refrigeration (MR) is the most advanced of all caloric technologies [2]; in particular, with the classes of magnetic refrigerants currently available, magnetocaloric refrigeration seems promising for applications in small temperature span (around 20 K), such as winecoolers and air conditioners [2].

In magnetic refrigeration, a *magnetocaloric material* (MCM) is subjected to a cyclical change of the applied magnetic field, and its temperature changes as a result of the *magnetocaloric effect* (MCE). The magnitude of the MCE depends on parameters related to characteristics of the material, magnetic field variation and temperature, and its maximal at the transition Curie temperature of the material. For a thorough introduction to the magnetocaloric effect and magnetocaloric materials, the reader is referred to [5].

Fábio P. Fortkamp
POLO — Research Laboratories for Emerging Technologies in Cooling and Thermophysics, Department of Mechanical Engineering, Federal University of Santa Catarina, Florianópolis, SC, 88040-900, Brazil, E-mail: fabio@polo.ufsc.br

Gusttav B. Lang · Jaime A. Lozano · Jader R. Barbosa Jr.
POLO — Research Laboratories for Emerging Technologies in Cooling and Thermophysics, Department of Mechanical Engineering, Federal University of Santa Catarina, Florianópolis, SC, 88040-900, Brazil

For operating conditions typical of a low-temperature span magnetic refrigerator, the MCE is typically on the order of 2-5 K. To amplify this temperature change, heat regeneration is usually employed [6]. Active magnetic regenerators (AMR) are thermal devices where the magnetocaloric material constitutes a solid matrix through which flows an aqueous heat transfer fluid, and is cyclically magnetized and demagnetized to activate the magnetocaloric effect. A regenerator is essentially a cascade of infinitesimal "layers" of MCM that are activated simultaneously to build up a temperature profile along its length. These layers can be made of the same material, yielding an homogeneous regenerator; however, given the dependence of the MCE with temperature, it is an interesting strategy to build *multilayer* regenerators, where each layer is composed of a different material that will work around its own Curie temperature, maximizing the magnetocaloric effect of each portion.

The five main subsystems in an AMR-based magnetic refrigerator can be identified as follows [7, 8]:

1. magnetic circuit;
2. active magnetic regenerator;
3. flow management system;
4. control system;
5. transmission system;
6. heat exchangers and cabinet.

The magnetic circuit generates oscillating magnetic fields that activate the MCE in the active magnetic regenerators. As previously explained, the regenerators are composed of magnetocaloric porous media, and the flow management system provides the alternating fluid flow through the beds. The control system serves the purpose of synchronizing the fluid flow regime with the magnetic field variations. Finally, the heat exchangers are responsible for transferring the cooling effect from the AMR to the refrigerated cabinet and the rejected heat to the surroundings.

Magnetic refrigerators can operate according to different thermodynamic cycles, but the stages are roughly as follows. The magnetic circuit magnetizes the MCM, increasing its temperature due to the MCE. During the so-called *cold blow*, cold fluid from the cold source flows through the warm bed and absorbs its energy, releasing it to the external heat exchanger. On the return of the fluid, the solid is demagnetized and cooled down, and in the *hot blow* the fluid relases energy to the bed, decreasing its temperature so it can absorb the thermal load at the cold source. The cycle then repeats; different cycles can be configured by different durations and synchronization steps between these two *characteristic waveforms*:

1. The *magnetic profile*, which describes the oscillating magnetic field over one regenerator;
2. The *fluid flow profile*, which describes the time-variation of flow rate through one bed.

Among the challenges cited in the literature for further improvement of magnetic refrigerators, two can be highlighted [9]:

1. Better use of AMR and magnetic circuit models during the design process, to identify optimal geometric and operating parameter;
2. Better study of losses that are present in a magnetic cooling device.

In other words, these challenges arise due to *interactions* between different subsystems of a magnetic refrigerator. In these context, the focus on the aforementioned waveforms is a suitable approach for optimizing the performance of magnetic refrigerators, as these profiles represent interactions between systems. As it will be seen, mathematical models for AMRs take these waveforms as input, and they are generated by models for other components.

Fluid flow profiles are more easily investigated with experimental methods, since they can be altered with modifications in the fluid flow system. In particular, the *duration* of blows have been extensively investigated [10, 11, 12], and the literature shows that the cooling capacity of magnetic refrigerators can be increased by focusing fluid flows during periods where the magnetic field is at its extrema values.

In this work, we focus on magnetic profiles, which are less studied in the literature. The studied waveforms are depicted in Figure 1, identified by the transitions between states. The instantaneous profile represents step-like changes between high and low levels of the magnetic field, while the ramp profile has linear variations between these states. The rectified cosine profile is a common waveform found in the literature that has a continuous variation of the applied magnetic field.

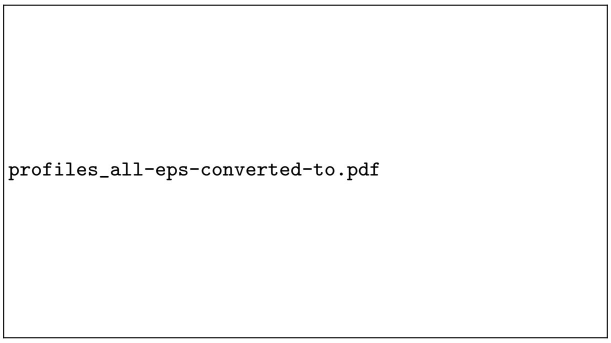

Fig. 1: Magnetic profiles studied in this paper

The instantaneous magnetic profile is characteristic of the Brayton AMR cycle, where the magnetization and demagnetization steps must be done adiabatically, as shown in Figure 2; compared to other common cycles such as the Ericsson, the Brayton cycle results in the highest cooling capacities for the same operating parameters [6], at the expense of lower coefficient of performance.

Fig. 2: Brayton AMR cycle

In practice, the ramp profile is a more feasible realization with finite transition times, and its synchronization with the fluid flow profile can yield different performance levels [13]. In particular, the plateaus of magnetic field should be centered with the blow durations [14]. Figure 3 shows the syncronization schema between the magnetic and fluid flow profiles, showing the ramp magnetic profile as an example.

This paper uses the AMR model developed by [15], and the same authors had studied magnetic profiles waveforms in an earlier work [16]. However, their amplitudes was not varied, nor were they investigated with different geometries.

The present works combines the gaps from the above cited papers in investigating the performance of a magnetic refrigerator under different magnetic profile waveforms. These

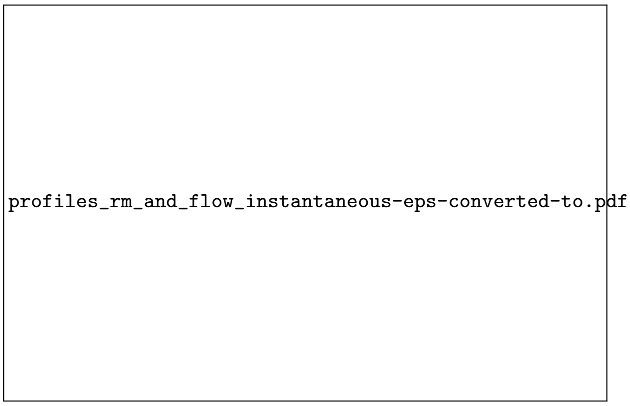

Fig. 3: Ramp magnetic profile (solid lines) and instantaneous fluid flow profile (dashed lines)

waveforms are mathematically modeled, and the cooling capacity and coefficient of performance are calculated based on the profiles parameters, while also investigated how the AMR geometry affect the performance in combinations with the magnetic profile. The fluid flow profile is assumed fixed in shape, although its parameters are also variied. The emulate constraints on an operating point of actual magnetic refrigeration devices, the temperature span is set fixed, and hence few comments are made on second-law efficiency.

2 Materials and methods

In this work, we perform numerical simulations of a previously developed AMR model, varying the profile and geometric parameters. We also couple a model for calculating the power comsumption of a proposed valve system, a topic understudied in the literature. With this, we can evaluate the influence of the profile on cooling capacity and coefficient of performance.

2.1 AMR model

2.1.1 Governing equations

Simulations were performed using a one-dimensional AMR mathematical model [16,15]. Here we will show a summarized version focusing on the governing equations. This model solves momentum and energy balance equations for the solid and fluid phases, represented by indices 's' and 'f', respectively. The model geometry is depicted in Figure 4, and assumes regenerators composed of monodisperse packed spheres with porosity ε.

The momentum equation for the fluid domain is:

$$\frac{\rho_\mathrm{f}}{\varepsilon}\frac{\partial V_z}{\partial t} = -\frac{\partial P}{\partial z} - \frac{\mu_\mathrm{f}}{K} V_z - \frac{c_\mathrm{E}\rho_\mathrm{f}}{K^{1/2}}\left|V_z\right| V_z \tag{1}$$

and is solved for the time-dependent uniform fluid velocity through the bed.

The energy equation for the fluid phase can be written as:

reg3d-eps-converted-to.pdf

Fig. 4: AMR model geometry

$$
\begin{aligned}
\rho_{\mathrm{f}} c_{p,\mathrm{f}} \left(\varepsilon \frac{\partial T_{\mathrm{f}}}{\partial t} + V_z \frac{\partial T_{\mathrm{f}}}{\partial z} \right) = & - \hbar_{\mathrm{sf}} \beta \left(T_{\mathrm{f}} - T_{\mathrm{s}} \right) \\
& + \left| V_z \left. \frac{\partial p}{\partial z} \right|_f \right| \\
& + \varepsilon \left(k_{\mathrm{f}}^{\mathrm{eff}} + \rho_{\mathrm{f}} c_{p,\mathrm{f}} D_{\mathrm{ld}} \right) \frac{\partial^2 T_{\mathrm{f}}}{\partial z^2} \\
& + \dot{q}_{\mathrm{csg}}
\end{aligned} \tag{2}
$$

while the energy equation for the solid phase is written as:

$$
\rho_{\mathrm{s}} c_{\mathrm{s}} (1-\varepsilon) \frac{\partial T_{\mathrm{s}}}{\partial t} = \hbar_{\mathrm{sf}} \beta (T_{\mathrm{f}} - T_{\mathrm{s}}) + (1-\varepsilon) k_{\mathrm{s}}^{\mathrm{eff}} \frac{\partial^2 T_{\mathrm{s}}}{\partial z^2} \tag{3}
$$

Initial and boundary conditions, solution methods, convergence analyses, and closure relations for the porous media terms are described in [15]. This AMR model solves the above equations for one regenerator operating between given sources temperatures, during one full cycle (hot and cold blows and magnetization and demagnetization periods), given specified operating conditions (to be discussed later).

The casing heat transfer term $\dot{q}_{\mathrm{csg}}$ in Equation 2 is calculated solving the heat conduction in the regenerators casing [15], and can be neglected to simplify some analyses. More details are provided in section 3.

2.1.2 How the fluid flow profile is used

The pressure gradient in Equation 1is modeled as:

$$
-\frac{\partial P}{\partial z} = \rho_{\mathrm{f}} A_{\mathrm{t}} g(t) \tag{4}
$$

where $g(t)$ is a dimensionless function that expresses the mathematical waveform of the pressure gradient, and A_{t} is its amplitude, adjusted in a convergence loop; the mass flow rate calculated from the Darcy velocity from Equation 1 is compared with the input value of mass flow rate until these values converge. The waveform $g(t)$ represents the fluid flow profile used.

2.1.3 How the magnetic profile is used

The magnetic profile is modeled by a waveform of magnetic field strength H applied perpendicular to the regenerators, as shown in Figure 4. The magnetic field is assumed uniform throughout the beds. The applied field is corrected from demagnetization effects to yield the effective field inside the regenerators:

$$H^{\mathrm{eff}} = H - N_{\mathrm{D}} M \tag{5}$$

where M is the magnetization field of the material, and N_{D} is a demagnetization factor.

The magnetocaloric effect is implemented in the so-called discrete approach [17]; every time the magnetic field changes, based on the input magnetic profile, the solid temperature is calculated according to:

$$T_{\mathrm{s}}(t+\Delta t) = T_{\mathrm{s}}(t) + \Delta T_{\mathrm{ad}}\left(T_{\mathrm{s}}(t), H^{\mathrm{eff}}(t), H^{\mathrm{eff}}(t+\Delta t)\right) \tag{6}$$

where the adiabatic temperature variation ΔT_{ad} is calculated from tabulated experimental data for magnetocaloric materials as function of temperature and effective field. [15].

2.1.4 Evaluation of solid and fluid properties

The fluid properties are considered constant in the momentum equation to decouple the solution procedures to determine the velocity and temperature fields. The properties are computed at the average temperature between the hot and cold sources temperatures, and are evaluated from interpolated tables exported from the EES software [18]. In all simulations shown in this work, the heat transfer fluid is a mixture of water/ethylene-glycol with concentration 80/20 % vol. For the energy equations, the fluid properties are also calculated from tabulated data, but the temperature dependence is considered.

n this chapter, all simulations use gadolinium or its allows as the magnetocaloric material. Gadolinium is a benchmark material with a Curie temperature of 290 K. For simplicity, the solid density is assumed constant at $\rho_{\mathrm{s}} = 7900\,\mathrm{kg/m^3}$ and the solid thermal conductivity is set to $k_{\mathrm{s}} = 10.5\,\mathrm{W/(m\,K)}$. The specific heat capacity of Gd is calculated as a function of temperature and magnetic field based on experimental data, using a bi-linear interpolation scheme; more details on the experimental dataset are available in [15].

In this work, both single- and multilayer regenerators are considered. For the multilayer simulations, alloys of gadolinium and yttrium are used in the form $\mathrm{Gd}_{1-x}\mathrm{Y}_x$, where x is the yttrium fraction. This fraction decreases the Curie temperature of the alloy relative to that of pure gadolinium. Due to the lack of experimental data on the magnetocaloric properties of $\mathrm{Gd}_{1-x}\mathrm{Y}_x$ alloys at the time this analysis was made, a simpler approach was used in which the properties of alloys with a low yttrium fraction are identical to those of pure gadolinium, except for the Curie temperature (which is shifted to lower values).

2.1.5 Performance metrics

The AMR model considers only one bed and assumes N_r identical beds experience the same cycle, multiplyind the performance metrics below by this factor

number of regenerators

The cooling capacity is calculated as [15]:

$$\dot{Q}_\mathrm{C} = N_\mathrm{r}\frac{1}{\tau}\int_{\tau_\mathrm{HB}} \dot{m}_\mathrm{f}(t) c_{p,\mathrm{f}} \left(T_\mathrm{C} - T_\mathrm{f,CE}\right) \mathrm{d}t \tag{7}$$

where τ is the cycle period, and τ_HB is the duration of the hot blow, during which the cold end temperature is compared to the cold source temperature.

The magnetic power to operate the AMR cycle is modeled as the ideal Carnot power, ignoring most thermal irreversibilities:

$$\dot{W}_\mathrm{mag} = \dot{Q}_\mathrm{C}\frac{T_\mathrm{H} - T_\mathrm{C}}{T_\mathrm{C}} \tag{8}$$

while the fluid friction irreversibility is accounted for in the calculation of the pumping power:

$$\dot{W}_\mathrm{pump} = N_\mathrm{r}\frac{1}{\tau}\int_0^\tau \frac{\dot{m}_\mathrm{f}}{\rho_\mathrm{f}} \Delta P \,\mathrm{d}t \tag{9}$$

where ΔP is the total pressure drop through the regenerator.

2.2 Hydraulic system and fluid flow profile model

The canonical fluid flow profile considered in this work is the square wave or *instantaneous profile*, because of the instantaneous change in flow rate, as shown in Figure 5.

The instantaneous mass flow rate, $\dot{m}_\mathrm{f}(t)$, is defined over a cycle with a period τ, and represents the fluid flow through a given regenerator bed. The so-called *hot cycle*, during which the MCM is magnetized, occupies the time interval $0 \le t < \tau/2$, while the *cold cycle* lies between $\tau/2 \le t \le \tau$. The flow profile oscillates between two plateaus of equal magnitude $\dot{m}_\mathrm{f,max}$ and opposite directions, which are centered in each half-cycle. During the hot cycle, the cold blow period is τ_CB, and during the cold cycle the hot blow period is τ_HB. If the flow is balanced, then $\tau_\mathrm{CB} = \tau_\mathrm{HB}$.

During each half cycle, there are periods without fluid flow, defined as:

$$\tau_\mathrm{0,HC} = \frac{\tau/2 - \tau_\mathrm{CB}}{2} \tag{10}$$

$$\tau_\mathrm{0,CC} = \frac{\tau/2 - \tau_\mathrm{HB}}{2} \tag{11}$$

where HC and CC stand for hot cycle and cold cycle, respectively.

The profile can be mathematically defined as:

$$\dot{m}_\mathrm{f}(t) = \begin{cases} 0, & 0 \le t < \tau_\mathrm{0,HC} \\ \dot{m}_\mathrm{f,max}, & \tau_\mathrm{0,HC} \le t \le \tau/2 - \tau_\mathrm{0,HC} \\ 0, & \tau/2 - \tau_\mathrm{0,HC} < t < \tau/2 + \tau_\mathrm{0,CC} \\ -\dot{m}_\mathrm{f,max}, & \tau/2 + \tau_\mathrm{0,CC} \le t \le \tau - \tau_\mathrm{0,CC} \\ 0, & \tau - \tau_\mathrm{0,CC} < t < \tau \end{cases} \tag{12}$$

mprofile-eps-converted-to.pdf

Fig. 5: Instantaneous fluid flow profile

When the blows have different time durations, the AMR cycle is considered unbalanced, and this is known to have a negative effect on performance [19, 11]. In this work, the blows are always balanced, hence the blow fraction, the ratio of blow durations to cycle period [11], can be evaluated as:

$$F_{\mathrm{B}} = \frac{2\tau_{\mathrm{B}}}{\tau} \tag{13}$$

where τ_{B} is the duration of one blow.

The hydraulic system to modulate this fluid flow through different regenerators at different time instants is composed of a pump and a set of electronic valves which can be precisely controlled to yield the desired blow durations. The electrical power consumed by the valve array is computed separately from other work contributions. An application of electronic valves in AMR devices has been presented by [20].

Due to evolving developments in our group, two types of valves are considered, as will be elaborated in section 3.

The first approach, called *Type B valves*, uses the model of [21], assuming that the individual consumption of each valve is independent of frequency and blow fraction. The valve power $\dot{W}_{\mathrm{valve}}$ can be computed as:

$$\dot{W}_{\mathrm{valve}} = N_{\mathrm{v}} F_{\mathrm{B}} \left(\dot{W}_{\mathrm{valve,n}} + \frac{1}{2} \dot{W}_{\mathrm{relay,n}} \right) \tag{14}$$

where N_{v} is the number of valves, $\dot{W}_{\mathrm{valve,n}}$ is the measured average nominal power for one normally-closed electronic valve and $\dot{W}_{\mathrm{relay,n}}$ is the nominal power for one controlling relay. The factor $1/2$ is due to two valves being controlled by one relay.

In the second approach, *Type A* valves are used, with lower nominal power but that depends on frequency and blow fraction. For these valves, the valve power was experimentally correlated as:

$$\dot{W}_{\mathrm{valve}}\,[\mathrm{W}] = N_{\mathrm{v}}\,(0.927f\,[\mathrm{Hz}] + 1.023F_{\mathrm{B}} + 0.226f\,[\mathrm{Hz}]F_{\mathrm{B}} - 0.037) \tag{15}$$

Equation (15) was correlated for blow fractions of 50 and 100 % and for frequencies in the range of 0.2–1.6 Hz, with an uncertainty on the order of 0.4 W for a single valve. The use of different valve types will be discussed among the presented results.

Indepedent of the valve type used, it is also assumed that this valve system can produce the fluid flow profile shown in Figure 5, where the displaced fluid mass during one blow in one regenerator bed is $\dot{m}_{\mathrm{f,max}} F_{\mathrm{B}} \tau/2$.

The *utilization factor* can then be calculated as:

$$\Phi = \frac{\dot{m}_{\mathrm{f,max}} F_{\mathrm{B}} c_{\mathrm{s}}}{2 f m_{\mathrm{s}} c_{\mathrm{s}}} \tag{16}$$

For an even number of poles in the magnetic circuit, it may be advantageous to employ an odd number of regenerator beds to break the symmetry between the magnetic circuit and the beds, thus avoiding positions of equilibrium between magnetic forces which result in torque oscillations [22]. Additionally, in general, two valves per regenerator may be necessary (one at each end), to independently control the hot and cold blows for each bed and correct flow imbalance; thus, in all results in this work, the number of valves is calculated as:

$$N_{\mathrm{v}} = 2N_{\mathrm{r}} \tag{17}$$

3 Results and Discussions

The simulated magnetic refrigerators are composed of multiple prismatic regenerators filled with gadolinium (Gd) spheres as the magnetocaloric solid matrix, with the parameters shown in Table 1. The fluid is a mixture of water and ethylene glycol, in the proportion of 80 %-20 % in volume.

Table 1: Geometric and operation parameters for the simulated AMR devices

Parameter	**Value**
Regenerator height	20 mm
Regenerator width	25 mm
Regenerator length	100 mm
Number of regenerators	11
Particle diameter	0.5 mm
Hot source temperature	298 K
Cold source temperature	278 K

3.1 Comparison of the instantaneous and rectified cosine profiles

When comparing the magnetic profiles, the average magnetic field during the hot cycle is the same; this implies in a higher peak for the rectified cosine. For the cold cycle, there are two possible comparison methods:

1. The minimum values for both profiles is the same;
2. The average value for both profiles during the cold cycle is the same.

As a reference, in all simulations the minimum value for the rectified cosine was fixed at $\overline{B}_{\mathrm{min,RC}} = 0.1\,\mathrm{T}$. For the first comparison, the minimum value for the instantaneous value was kept at the same level ($\overline{B}_{\mathrm{min,I}} = \overline{B}_{\mathrm{min,RC}}$), hence, the average low value for the RC profile was higher ($B_{\mathrm{l,RC}} > B_{\mathrm{l,I}}$). Although this does not seem a fair comparison, in practice it is feasible to generate a profile with a constant low-valued plateau for the magnetic field [23,24]. For the other comparison method, the low level of the instantaneous profile was increased ($\overline{B}_{\mathrm{min,I}} > \overline{B}_{\mathrm{min,RC}}$) to keep the average the same ($B_{\mathrm{l,RC}} = B_{\mathrm{l,I}}$). In addition, simulations were ran for various values of blow fraction and the optimal cases were selected; the rectified cosine profile can benefit from a smaller blow fraction because this can concentrate the flow during the periods of very high or low fields. In this section, all results show the resulting optimal case of the blow fraction for each profile (for the values tested): fluid flowing during the entire period for the instantaneous profile, and only during 60 % of the period for the cosine profile.

Figure 6 shows the cooling capacity attained by the device at a frequency of 1 Hz and different utilizations, for both comparison methods. The horizontal axis shows the average value during the high field region. Notice how the results are conflicting; for Fig. **??**, the instantaneous profile almost always yields a higher performance, while for Fig. **??** the rectified cosine profile generates higher cooling capacities. Since the average during the hot cycle (high field stage) is the same, the main difference is due to the low magnetic field levels. For the "same minimum" comparison, the instantaneous profile is capable of keeping the magnetic field at low levels for the whole half-cycle, which is beneficial for performance; for $\Phi = 1.0$ and $B_{\mathrm{h}} = 1.40\,\mathrm{T}$, the cooling capacity for the instantaneous profile is 196.3 % higher than for the cosine profile. As demonstrated by [16], a higher average magnetic field during the low-field stage increases the solid temperature and consequently results in warmer fluid entering the cold heat exchanger, representing a thermal loss. In the "same-average" comparison, the cosine profile is capable of achieving much lower levels (since its minimum value is fixed), therefore providing more cooling power. However, as explained before, it is possible to design near-instantaneous profiles with very low levels of the magnetic field.

Fig. 6: Cooling capacity as a function of the average high magnetic field, for different utilizations. "I": instantaneous (blow fraction of 100 %); "RC": rectified cosine (blow fraction of 60 %), for both comparison methods.

The only exception in the "same minimum" comparison is seen for the lowest utilization of $\Phi = 0.2$, where the performance is slightly better for the RC profile. Since the blow fraction for the cosine is lower, the mass flow rate must be higher to yield the same utilization (cf. Eq. (**??**)), and this increases heat transfer rate, as previously explained — outweighing the effects of the magnetic field.

In general, the performance of the AMRs operating with the instantaneous magnetic profile yields better results. As can be seen on Fig. 6, an instantaneous profile with the lowest possible value of B_{min} and the highest possible value of B_{max}, with a flow profile occupying the whole cycle with average values of utilization, results in the highest values of cooling capacity among all simulations, therefore, representing the ideal magnetic profile for an AMR.

3.2 Analysis of the instantaneous profile

As shown in the previous section, the instantaneous profile yields the highest values for cooling capacity. Therefore, in this section, a more detailed analysis of such profile has been carried out. Figure 7 shows the cooling capacity as function of utilization, for several levels of the maximum magnetic field for the instantaneous profile, for two different operating frequencies. Because of the conflicts between a low heat transfer rate for flow rates too low and a loss in regenerator effectiveness in flow rates too high, there are critical values of utilization that maximize cooling capacity, and this critical value grows with the level of magnetic field. With higher magnetic field, the increase in the MCE surpasses the loss of effectiveness, and one can go to higher flow rates without losing performance. It can also be seen in Fig. 7 that at higher frequencies, the values of cooling power are higher, and also the critical values of utilization are lower; however, this usually is achieved at the cost of higher power consumption in AMR devices at higher frequencies [25, 26].

Qc_Phi_inst_f_1_Hmin_005_FB_100-eps-converted-to.pdf

(a) $f = 1\,\mathrm{Hz}$

Qc_Phi_inst_f_2_Hmin_005_FB_100-eps-converted-to.pdf

(b) $f = 2\,\mathrm{Hz}$

Fig. 7: Cooling capacity as a function of utilization, for various values of the high magnetic field of the instantaneous profile

The parameters in Table 1 were chosen from preliminary simulations, but they are not guaranteed to be the optimal choices. To understand the impact of regenerator geometry on the performance with the instantaneous profile, the regenerator height was varied in Fig. 8, Qc_H_inst_f_1_Phi_40-eps-converted-to.pdf

Fig. 8: Cooling capacity as a function of regenerator height (all other parameters from Table 1 constant) for various values of the high magnetic field of the instantaneous profile

and all other parameters from Table. 1 were kept fixed. As expected, higher magnetic fields allow for smaller regenerators (and hence more compact systems). For instance, to achieve a capacity of 100 W, increasing the field from 1.0 to 1.2 T result in using regenerators 36 % smaller.

4 CONCLUSIONS

A one-dimensional AMR numerical model was used to compare the performance of a magnetic refrigerator under different operating and geometric parameters and with the instantaneous and rectified cosine magnetic profiles. Most of the AMRs operating with an instantaneous magnetic profile have resulted in better performances than those with a cosine profile, except in cases of low utilization. Although the cosine profile reaches higher levels of the magnetic field, the instantaneous profile can keep the magnetization (and demagnetization) for a longer period, which is shown to be beneficial to performance. Further analysis of the instantaneous profile has shown that the use of the highest possible value of the maximum magnetic field allows for using smaller regenerators and lower utilization, without losing performance.

Acknowledgements This work was supported by CNPq, Embraco and EMBRAPII Unit Polo/UFSC.

References

1. P. Bansal, E. Vineyard, O. Abdelaziz, International Journal of Sustainable Built Environment **1**, 85 (2012)
2. A. Kitanovski, U. Plaznik, U. Tomc, A. Poredoš, International Journal of Refrigeration **57**(Supplement C), 288 (2015). DOI https://doi.org/10.1016/j.ijrefrig.2015.06.008
3. IIR. 36th informatory note on refrigeration technologies: Flammable refrigerants. Available at `http://www.iifiir.org/userfiles/file/publications/notes/NoteTech_36_EN_nkyix2fcj7.pdf` (2017). Accessed on October 30th, 2018
4. S. Lionte, M. Risser, C. Vasile, L. Elouad, C. Muller, International Journal of Refrigeration **85**, 303 (2018). DOI 10.1016/j.ijrefrig.2017.10.009
5. A. Smith, C.R.H. Bahl, R. Bjørk, K. Engelbrecht, K.K. Nielsen, N. Pryds, Advanced Energy Materials **2**, 1288 (2012)
6. A. Kitanovski, U. Plaznik, J. Tušek, A. Poredoš, International Journal of Refrigeration **37**, 28 (2014)

7. J.A. Lozano, Cadena, Designing a rotary magnetic refrigerator. Mechanical Engineering, Federal University of Santa Catarina, Florianópolis (2015)
8. P.V. Trevizoli, T.V. Christiaanse, P. Govindappa, I. Niknia, R. Teyber, J.R. Barbosa, Jr., A. Rowe, Science and Technology for the Built Environment **22**(5), 507 (2016). DOI 10.1080/23744731.2016.1171632
9. D. Eriksen, Active magnetic regenerator refrigeration with rotary multi-bed technology. Department of Energy Conversion and Storage, Technical University of Denmark, Denmark (2016)
10. R. Teyber, P.V. Trevizoli, I. Niknia, T.V. Christiaanse, P. Govindappa, A. Rowe, International Journal of Refrigeration **74**, 38 (2017)
11. A.T.D. Nakashima, S.L. Dutra, P.V. Trevizoli, J.R. Barbosa, Jr., International Journal of Refrigeration **93**, 236 (2018)
12. F.P. Fortkamp, D. Eriksen, K. Engelbrecht, C.R.H. Bahl, J.A. Lozano, J.R. Barbosa, Jr., International Journal of Refrigeration **91**, 46 (2018). DOI 10.1016/j.ijrefrig.2018.04.019
13. J. Tušek, A. Kitanovski, I. Prebil, A. Poredoš, International Journal of Refrigeration **34**(6), 1507 (2011). DOI 10.1016/j.ijrefrig.2011.04.007
14. R. Bjørk, K. Engelbrecht, International Journal of Refrigeration **34**, 192 (2011). DOI 10.1016/j.ijrefrig.2010.07.004
15. P.V. Trevizoli, A.T. Nakashima, J.R. Barbosa, Jr., International Journal of Refrigeration **72**(206-217) (2016)
16. P.V. Trevizoli, J.R. Barbosa, Jr., A. Tura, D. Arnold, A. Rowe, Journal of Thermal Science and Engineering Applications **6** (2014)
17. K.K. Nielsen, J. Tusek, K. Engelbrecht, S. Schopfer, A. Kitanovski, C.R.H. Bahl, A. Smith, N. Pryds, A. Poredos, International Journal of Refrigeration **34**, 603 (2011)
18. S.A. Klein. EES — Engineering Equation Solver, Professional Version v9.339. F-Chart Software (2013). Available at `http://fchart.com`.
19. D. Eriksen, K. Engelbrecht, C.R.H. Bahl, R. Bjørk, K.K. Nielsen, Applied Thermal Engineering **103**, 1 (2016)
20. A.T.D. Nakashima, S.L. Dutra, G. Hoffmann, J.A. Lozano, J.R. Barbosa, Jr., in *Proceedings of the 8th International Conference on Caloric Cooling (Thermag VIII)* (Darmstadt, Germany, 2018)
21. P.O. Cardoso, M.C. Destro, M.G. Alvarez, J.A. Lozano, J.R. Barbosa, Jr., V.J. de Negri, in *Proceedings of the 16th Brazilian Congress of Thermal Sciences and Engineering* (Vitória, 2016)
22. D. Eriksen, K. Engelbrecht, C.R.H. Bahl, R. Bjørk, K.K. Nielsen, A.R. Insinga, N. Pryds, International Journal of Refrigeration **58**, 14 (2015)
23. A.R. Insinga, Optimising magnetostatic assemblies. Department of Energy Conversion and Storage, Technical University of Denmark (2016)
24. M.A. Benedict, S.A. Sherif, D.G. Beers, M.G. Schroeder, Science and Technology for the Built Environment **22**(5), 520 (2016). DOI 10.1080/23744731.2016.1185889
25. T. Lei, K. Engelbrecht, K.K. Nielsen, C.T. Veje, Applied Thermal Engineering **111**, 1232 (2017)
26. I. Niknia, O. Campbell, T.V. Christiaanse, P. Govindappa, R. Teyber, P.V. Trevizoli, A. Rowe, Applied Thermal Engineering **106**, 601 (2016). DOI 10.1016/j.applthermaleng.2016.06.039